frontiers | Frontiers in Materials

TYPE Original Research
PUBLISHED 10 April 2023
DOI 10.3389/fmats.2023.1165971

OPEN ACCESS

EDITED BY
Sheng Guo,
Chalmers University of Technology, Sweden

REVIEWED BY
Liuliu Han,
Max-Planck-Institut für Eisenforschung, Germany
Junyang He,
Central South University, China

*CORRESPONDENCE
Haoran Fu,
Fuhr@zju.edu.cn
Hua Wei,
huawei@zju.edu.cn

SPECIALTY SECTION
This article was submitted to Structural Materials, a section of the journal Frontiers in Materials

RECEIVED 14 February 2023
ACCEPTED 24 March 2023
PUBLISHED 10 April 2023

CITATION
Xie Y, Zhao J, Fu H and Wei H (2023), Dependence of microstructural evolution on the geometric structure for serviced DZ125 turbine blades.
Front. Mater. 10:1165971.
doi: 10.3389/fmats.2023.1165971

Dependence of microstructural evolution on the geometric structure for serviced DZ125 turbine blades

Yadan Xie[1,2], Jianjiang Zhao[1,3], Haoran Fu[1,3]* and Hua Wei[1,3]*

[1]Center of Hypergravity Experimental and Interdisciplinary Research, Zhejiang University, Hangzhou, Zhejiang, China, [2]Center of Electron Microscopy and State Key Laboratory of Silicon Materials, School of Materials Science and Engineering, Zhejiang University, Hangzhou, Zhejiang, China, [3]College of Civil Engineering and Architecture, Zhejiang University, Hangzhou, China

The turbine blades were directionally solidified by a high-rate solidification process by the Bridgman technique using directional solidified Ni-based master superalloy DZ125 and operated on the engine bench with a high-temperature gas environment of more than 1500 °C from combustor and high-speed rotation of more than 13500 rpm for 400 h. A service-environment-based model was put forward to simulate the distribution of temperature and stress on the DZ125 blade in service. It was found that the distribution of temperature and stress on the serviced DZ125 blade was closely related to its geometric structure. The microstructural evolution of the serviced DZ125 blade was analyzed and the variations of microstructures with temperature and stress were investigated by using a scanning electron microscope. The results revealed that the evolution process of microstructures on the serviced DZ125 blade was different from that of the standard sample tested at constant temperature and uniaxial tensile stress. The reason for this discrepancy was explored using a combination of finite-element calculation and diffusion coefficient calculation.

KEYWORDS

turbine blade, microstructural evolution, high-speed rotation, high temperature, diffusion

1 Introduction

Gas turbine is one of the most efficient heat-to-power conversion machinery and widely used in aero-engines. In the service of gas turbines, the integrity of turbine blades as a core component of aero-engines is of great importance to the service safety (Rogge et al., 2018). In addition, temperature and centrifugal stress on turbine blades change sharply during take-off, cruise, and landing of aircrafts. Because of these, as the key aerodynamic part responsible for the energy transformation in gas turbines, turbine blades are always manufactured by advanced superalloys. It should be known that turbine blades work at various speeds and temperatures, and it leads to turbine blades subjected to a wide range of temperature and stress produced by high-temperature gas from the combustion chamber and high-speed rotation in service (Zadvorniy et al., 2015).

The directional solidified (DS) superalloy DZ125 exhibits columnar crystalline morphology with the <001> orientation, which is parallel to the centrifugal stress of blades (Chen et al., 2020). Compared with polycrystalline and wrought superalloys, the

DZ125 superalloy can render superior microstructural stability and mechanical properties at elevated temperatures due to the elimination of undesirable transverse grain boundaries (Fu et al., 2020). The DZ125 superalloy also possesses exceptional elevated temperature strength, high resistance to creep, no obvious thin-wall effect, good oxidation and corrosion resistance, as well as good fracture toughness and is widely employed in manufacturing high-pressure turbine blades (Pollock and Argon, 1994;Duscher et al., 2004; Chellali et al., 2016). A large amount of experimental and theoretical studies regarding the DZ125 superalloy were conducted to explore the relationship between mechanical properties and the γ–γ′ microstructural degradation (Cottura et al., 2012; Fedelich et al., 2012; Sadowski and Golewski, 2012; Cottura et al., 2016; Barba et al., 2018). Understanding the failure mechanism and predicting creep lifetime have been a long-term requirement in order to ensure the flight safety of engines. In this respect, macroscopic methods, e.g., macroscopic constitutive modeling, are insufficient mainly because the plastic deformation takes place at external stress far below macroscopic yield stress according to the classic strength theory, but the microstructural degradation of the DZ125 superalloy under high-temperature and low-stress conditions is observed experimentally. The DZ125 superalloy mainly consists of channel-like γ phase and cuboid γ′ phase surrounded by the matrix γ phase. Operating at a high-temperature and high-speed rotating state, the DZ125 superalloy strengthened by γ′ precipitates inevitably experiences the microstructural degradation, mainly including coarsening, connection, dissolution, and rafting of γ′ precipitates (Fu et al., 2019; Fu et al., 2020), and finally results in blade failure.

In recent years, investigations on γ′ precipitates degradation were extensively carried out and many models for coarsening and rafting of γ′ precipitates were proposed and well applied for DS superalloys (Ichitsubo et al., 2003; Dye et al., 2008; Takahashi et al., 2008). Recent decades have seen an increasing interest in estimating the remaining creep lifetimes of turbine blades as a means of ensuring the safety of engines. Gan et al. (2020) introduced the initial damage terms that are related with the topologically close-packed (TCP) phase and the coarsen γ′ precipitates when predicting the remaining lifetime. Tian et al. (2011) considered the micropores in the lifetime prediction model. These reported results can predict the residual lifetime well when applied to standard samples; Huang et al. (2022) used smooth and three types of U-shape single-edge notched plate specimens to investigate stress rupture behavior of the DZ125 superalloy. A combined creep-viscoplasticity constitutive model was employed to analyze the distribution of stress and strain near the notch root. The results indicated that the different stress distribution and creep restraint between asymmetric notched plate specimens and symmetric notched round bars are the main reasons for the corresponding failure mechanism; Wang et al. (2021) used a combination of hot isostatic pressing (HIP) and rejuvenation heat treatment (RHT) technology to restore creep-damaged DZ125 superalloy and then studied the influence of microstructural restoration on the high-temperature fatigue property of the DZ125 superalloy. The results showed that the HIP + RHT process could effectively heal internal cavities and recover the degraded γ′ phase in creep-damaged DZ125 superalloy to the initial cubic-like particles. However, due to the complex geometrical structure and service conditions of turbine blades, it is questionable that the lifetime evaluation method by the microstructure of the standard samples in the lab can be directly used for the service-exposed turbine blades. Holländer et al. (2016) studied the effect of service-induced microstructural degradation on the tensile and fatigue properties of two service-exposed industrial gas turbine blades using small-scale samples, revealing that the microstructural degradation in the air foil section has a detrimental effect on the fatigue resistance. It should be noted that investigations of the turbine blade material for actual service mostly focus on the establishment of the damage evaluation criteria for blades (Holländer et al., 2016; Tong et al., 2016; Wang et al., 2021). In their work, the microstructure of the material under different conditions, for which the stress applied is surface force (e.g. uniaxial tensile stress), was obtained and then quantitatively characterized as the characteristic parameters of the material under the specific temperature and stress (Guo et al., 2019a). In this way, the service condition of the blade was obtained by comparing the characteristic parameters of the microstructure on blades with the standard sample. It is clear that the diversity of the degradation mechanism of the microstructures between blades and the standard samples was ignored, and thus, the rationality of comparing the blades and the standard samples was rarely discussed. Nevertheless, the difference must exist because of the uncertainty of service history and the complexity of temperature and stress distribution for turbine blades exposed to a combined environment of high-temperature gas and high-speed rotation.

In fact, the actual service conditions of turbine blades is a coupling environment of non-isothermal and high-speed rotation. It is quite different from the isothermal and uniaxial stress of the standard sample in the laboratory, and airworthiness authorities (e.g., FAA in the United States and EASA in Europe) require turbine blades to undergo the special experiments to simulate the actual service conditions. Rowe and Freeman (1961) investigated the overheating service degradation of the M252 superalloy to explore the effect of the higher abnormal operational temperature, which is referred to as overheating service (Dye et al., 2008), on creep property. Zhao et al. (2022) investigated the role of oxidation and recrystallization on very-high-cycle fatigue of the DZ125 superalloy at a temperature from 850 to 1000 °C because very-high-cycle fatigue is the most important failure mode of turbine blades in modern engines. Therefore, it is of critical importance to directly study the failure mechanism of turbine blades under the simulated engine operating conditions to the greatest extent.

It is well known that temperature and stress are two crucial factors that influence the microstructural degradation of Ni-based superalloys (Kakehi, 1999; Maldini et al., 2007; Yue et al., 2019). To be more specific, temperature is a scalar while stress is a vector. When testing the creep property of the materials at constant temperature in the laboratory, the applied axial stress is the surface force. The stress that turbine blades bear when rotating at high speed is the inertial force or body force, which is a function of the material density and the distance to the rotation center. It can be predicted that different stress loading methods of the surface force and the body force may affect the microstructure and mechanical properties of the materials in different ways when testing the

mechanical properties of the same materials at the same temperature.

In our work, a turbine blade with the film cooling holes was manufactured by the DZ125 superalloy and in service on the engine bench with a high-temperature gas environment of more than 1500 °C from combustor and high-speed rotation of more than 13500 rpm for 400 h. A service-environment-based model was put forward to simulate distribution of temperature and stress on blades in service. The service-induced microstructural degradation of the DZ125 blade was analyzed and the variations of microstructures with temperature and stress were investigated by a scanning electron microscope. The service-induced microstructural degradation of the DZ125 blade is in the way different from that of the standard sample tested at constant temperature and uniaxial tensile stress. The reason for this discrepancy was explored using a combination of finite-element calculation and diffusion coefficient calculation.

2 Experimental and methods

2.1 Experimental

The DZ125 turbine blades were directionally solidified by a high-rate solidification (HRS) process with a 3.5 mm/min withdrawal rate by the Bridgman technique at the AECC Beijing Institute of Aeronautical Materials. The DZ125 blades were subsequently subjected to the standard heat treatment: 1180 °C/2 h + 1230 °C/3 h with air cooling (AC) + 1100 °C/4 h (AC) + 870 °C/20 h (AC). The chemical composition of the DZ125 superalloy is Ni-8.9% Cr-10% Co-7% W-2% Mo-5.2% Al-0.9% Ti-0.8% Ta-1.5% Hf (wt%). In order to simulate the geometric structure of the turbine blade body as much as possible, the film cooling holes (FCHs) of the heat-treated DZ125 blades were perforated by using an electrical discharge machine (EDM, Rotary Electro-Discharge Grinder, ZGD703C) and then drilled by the high-speed electric spark machining method in strict accordance with the processing technology of FCHs at AVIC Manufacturing Technology Institute. The surface quality of the FCHs is fine. The inner wall roughness of the FCHs drilled is uniform. The DZ125 blades with the film cooling holes operate on the engine bench with the high-temperature gas environment of more than 1500 °C from combustor and high-speed rotation of more than 13500 rpm for 400 h. In order to compare with the service-induced microstructure at the typical locations on the DZ125 blade, the specimen cut from the blade rabbet is considered to be the original microstructure.

The specimens were cut from the interested locations of the blade for the observation of γ′ precipitates. Metallographic specimens were mechanically polished and then electrolytically etched using 2% H_3PO_4, 40% HNO_3, and 48% H_2SO_4 electrolyte solution with a voltage of 3 V for about 30 s. The γ/γ′ phase examination was performed using a SU-70 field-emission scanning electron microscope (FE-SEM). Diffraction measurements were performed by X-ray diffraction (XRD, X' Pert PRO) to obtain the lattice parameters of the γ and γ′ phases. Using multiple images for statistical purposes, the quantitative analysis of the microstructural degradation included the characterization of the volume fraction of the γ′ phase (V_f) and thickness of the rafted γ′ precipitates (D). It should be noted that V_f is replaced by the area fraction in each SEM image and D is defined as the width of the γ′ precipitates.

2.2 Temperature field model of the blade

In order to simulate temperature distribution of the cross sections on the DZ125 blade in service, the temperature field model was put forward on the basis of the overall energy continuity across the blade with the consideration of heat transfer between hot gas traversing the blade and cooling air passing through a cooling channel inside the blade from blade root to blade tip. The cooling air usually comes from the exit of the upstream compressor. According to the study of Saturday et al. (2017), a radial temperature distribution along the blade height is given in Figure 1. It can be seen that temperature along the blade height continuously increases from the root, reaches the maximum at the middle of the blade, and then decreases gradually. Clearly, the maximum temperature occurs at the middle of the blade (B point) while the minimum temperature occurs at the root (A point) and the tip (C point) of the blade. To simplify the model, temperature from B point to A point and C point of the blade, separately, can be approximately linear with the blade height (Shi et al., 2013). To decrease the working temperature of the turbine blade surface, several rows of film cooling holes are machined on the blade body. During the operation, the cooling gas flowing from the holes can form a thin layer of air-cooled film on the blade surface so as to avoid the heat transfer between the high-temperature gas and the blade directly. Under the ideal conditions, the blade surface is adiabatic without heat exchange with the air-cooled film. The cooling efficiency of the air-cooled film, η_f, can be expressed (Eshati et al., 2013) as $\eta_f = \frac{T_g - T_{aw}}{T_g - T_{c,in}}$, where T_g is the gas temperature, T_{aw} is the blade surface temperature related with the distance to film cooling holes, and $T_{c,in}$ is the inlet temperature of the cooling gas. Under the practical condition, heat conduction exists between high-temperature gas and air-cooled films on the blade surface. It means that temperature of air-cooled film achieves the thermal balance with the blade surface temperature. Assuming that q_0 is the total heat flow from the high-temperature gas and q_w is the heat flow to the blade wall, the heat taken away by air-cooled films can be expressed (Liu et al., 2010) as $\Delta q = q_0 - q_w = h_0 (T_b - T_{aw})$, where h_0 is the heat transfer coefficient of the blade wall. We obtain the expression of the blade wall temperature T_b as follows (Liu et al., 2010):

$$T_b = \frac{\Delta q}{h_0} + T_{aw} = \frac{\Delta q}{h_0} + \left[T_g - \eta_f (T_g - T_{c,in})\right]. \quad (1)$$

Here, we assume that gas temperature T_g and the inlet temperature of the cooling gas $T_{c,in}$ are constants. η_f can be regarded as a linear function of the distance to film cooling holes x (Sinha et al., 1991; Sen et al., 1996). T_{aw} is a linear function of the distance to film cooling holes x. The slope of the $T_{aw} - x$ curve can be estimated as $k_{T_{aw}-x}$. In Eq. (1), Δq can also be seen as the increment of the heat when the cooling gas flows downstream, which is related with the variation of temperature from the film cooling holes to the downstream. We obtain $\Delta q = h\Delta T_{aw} = h \cdot k_{T_{aw}-x} \cdot x$, where h is the heat transfer coefficient of the cooling gas. Consequently, the temperature of the blade wall T_b can be expressed as

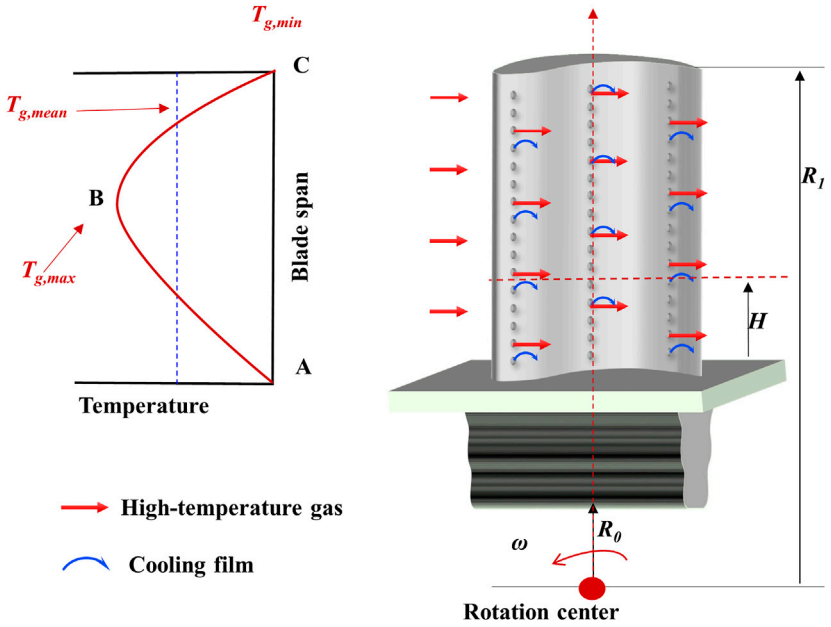

FIGURE 1
Schematic of the model assisted in calculating the temperature and stress distribution of the DZ125 blade in service.

$$T_b = \frac{hk_{T_{aw}-x}x}{h_0} + T_{aw} = \frac{hk_{T_{aw}-x}x}{h_0} + \left[T_g - \eta_f\left(T_g - T_{c,in}\right)\right], \quad (2)$$

where T_{aw}, h_0, T_g, and $T_{c,in}$ are known when the DZ125 blade is in service.

2.3 Stress distribution model of the blade

In order to simulate stress distribution of the cross sections on the DZ125 blade in service, the stress distribution model was built considering the centrifugal force derived from the blade rotation. The centrifugal force F_i generated by each blade section is calculated by $F_i = m_i \times \omega^2 \times h_i$, where m_i is the mass of the section, ω is the angular speed of rotation, and h_i is the distance from the center of gravity of each section to the turbine axis of rotation. The centrifugal stress at each section, σ_i, is given by $\sigma_i = F_i/A_i$, where A_i is the area of each blade cross section. In service, high-temperature gas flow velocity changes simultaneously in both the axial and the tangential directions. It implies that in axial and tangential velocity bending moment about the center of gravity of each blade section is relatively stable. The static pressure difference between the suction and pressure sides of the blade is small compared with the centrifugal force. The bending moment stresses produced by pressure difference and velocity difference along the blade height is, thus, ignored and the centrifugal stresses on the section are taken into considered in our model. As shown in Figure 1, assuming that the area of the cross section of the blade remains unchanged with the height, the centrifugal stresses on the section at height H is given by

$$\sigma_C(H) = \omega^2\rho \cdot \left(-\frac{1}{2}H^2 - 2R_0H - \frac{3}{2}{R_0}^2 + \frac{1}{2}{R_1}^2 + R_0R_1\right), \quad (3)$$

TABLE 1 Parameters used in the temperature field model and the stress field model.

$T_{g,max}$	1700 °C
$T_{g,min}$	1500 °C
$T_{c,in}$	500 °C
H_{max}	400 mm
H/H_0	0.85
ω	1413 rad/s
ρ	8.15 g/cm^3
R_0	318.4 mm
R_1	358.4 mm

where ρ is the density of the DZ125 blade, R_0 is the distance between the root of the blade and the rotation center, and R_1 is the distance between the tip of the blade and the rotation center. These parameters are known when the DZ125 blade is in service.

3 Results

3.1 Temperature and stress distribution on the blade

The temperature distribution of the blade wall, especially along the radial and longitudinal direction of the blade in service, is mainly decided by gas temperature and distribution of film cooling holes in

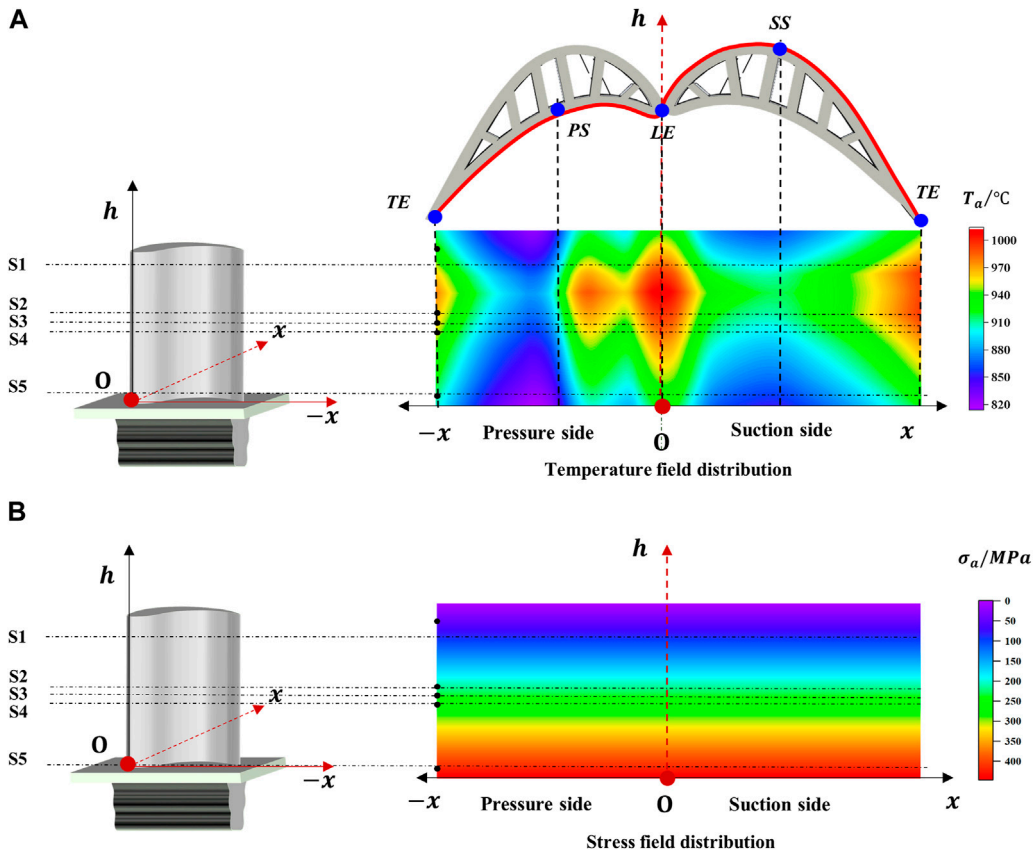

FIGURE 2
Temperature and centrifugal stress profiles of the DZ125 blade in service. **(A)** Temperature distribution of the DZ125 blade wall with film cooling holes and **(B)** centrifugal tensile stress distribution along the blade height.

TABLE 2 Temperature and stress at different locations of the blade.

	S5		S4		S3		S2		S1	
	T/°C	*σ*/MPa	*T*/°C	*σ*/MPa	*T*/°C	*σ*/MPa	*T*/°C	*σ*/MPa	*T*/°C	*σ*/MPa
LE	930	445.3	1000	264.9	1000	231.6	1000	198.1	990	113.9
SS	870	445.3	900	264.9	910	231.6	920	198.1	900	113.9
PS	870	445.3	870	264.9	890	231.6	890	198.1	870	113.9
TE	930	445.3	950	264.9	960	231.6	970	198.1	940	113.9

the blade body. The temperature field model and the stress field model are used to calculate temperature and stress distribution of the blade wall in service. Table 1 gives the parameters used in the models. The calculated results by Eqs. 2, 3 are shown in Figure 2 and Table 2. Figure 2A indicates that the temperature distribution of the blade wall is abruptly inhomogeneous along the radial direction on a longitudinal section. On any longitudinal section, the temperature at the leading edge (LE) and the trailing edge (TE) of the blade is the highest while the temperature at the pressure side (PS) and the suction side (SS) is relatively low and about lower than 850 °C. Temperature near the blade tip is approximately comparable to that near the blade root. The typical characteristic of stress distribution in Figure 2B is linearly gradient along the longitudinal direction and the centrifugal stress level is equivalent on any radial section. The centrifugal stress gradient along the longitudinal direction is about 11 MPa/mm, and the temperature gradient from the blade root to the upper middle part of the blade is about 3–5 °C/mm.

It was found in Figure 2 that the temperature and stress distribution on the DZ125 blade exposed to a combined environment of high-temperature gas and high-speed rotation were closely related to the geometric structure. The coupling of temperature and stress has a significant influence on the morphological evolution of γ′ precipitates and γ matrix of the DZ125 blade. In order to examine the microstructural degradation of the blade after service, the typical locations of the blade are selected to assess the microstructural degradation degree of the blade based on the calculated temperature and stress field distribution. Because there is a big difference in temperature and stress between the radial and longitudinal section,

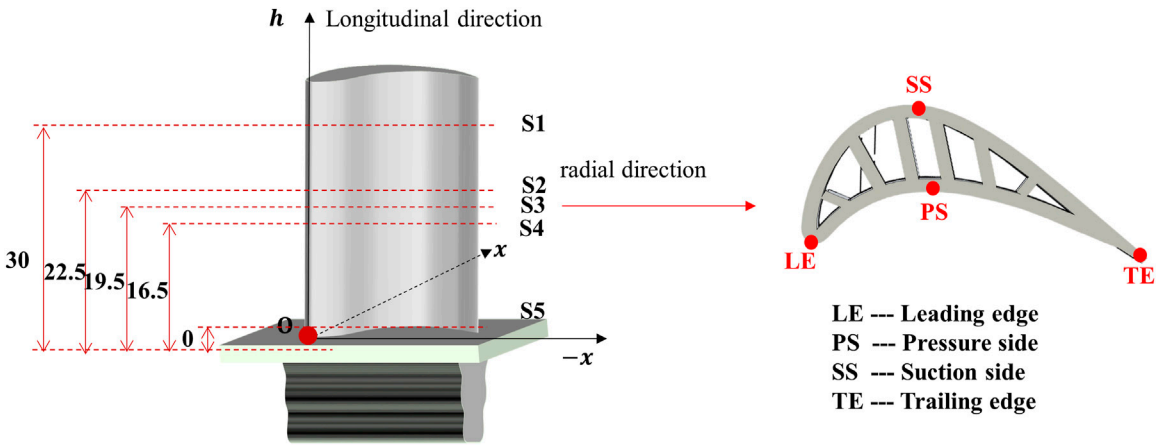

FIGURE 3
Selected locations of the observation points on each section.

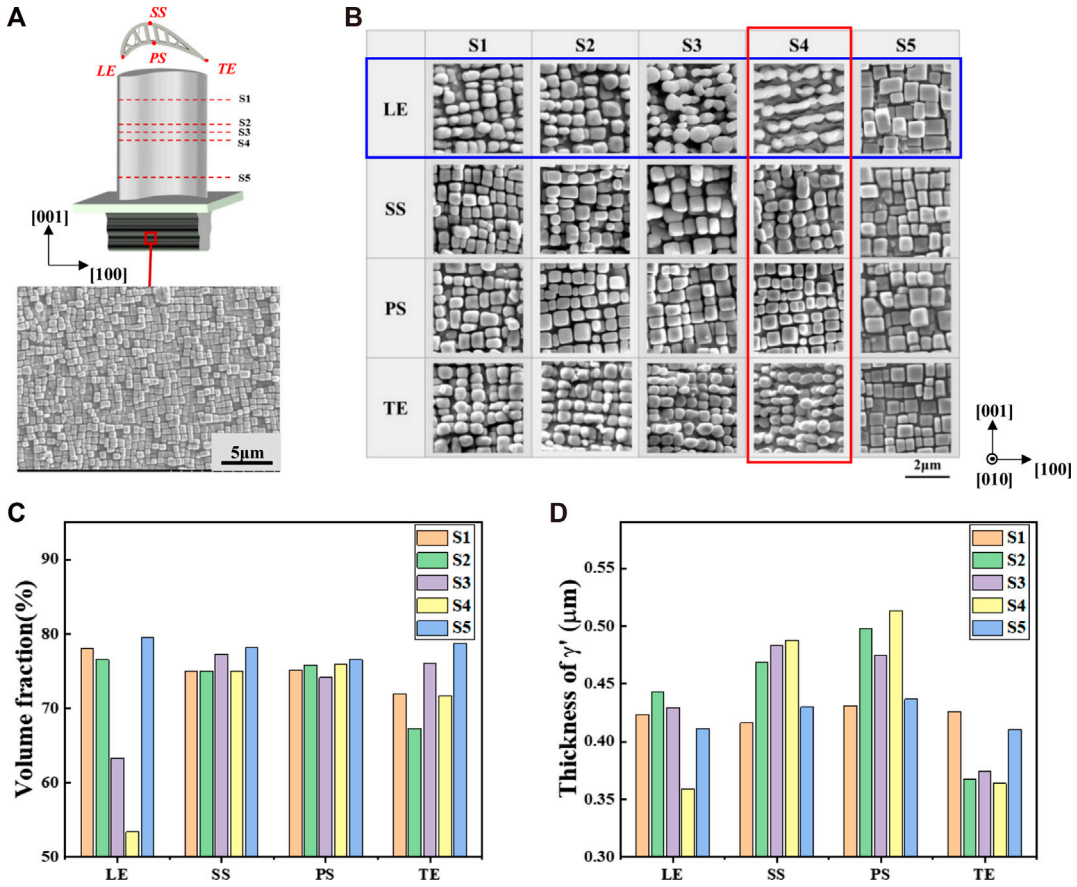

FIGURE 4
(A) Morphology of the DZ125 blade rabbet, **(B)** microstructural evolution of the selected locations on the serviced DZ125 blade, and **(C, D)** volume fraction and thickness of γ′ precipitates at different locations of each section on the serviced DZ125 blade.

as shown in Figure 3, the five representative cross sections and the four typical locations at each cross section are chosen for assessment of the microstructural degradation of the DZ125 blade. Among the selected cross sections as shown in Figure 3, section 1 (S1) is close to the blade tip and corresponds to medium temperature and low stress, section 5 (S5) is near the blade root, corresponding to low temperature and high stress, and section 2, section 3, and section 4 (S2, S3, and S4) are taken at the middle height of the blade and the distance between each section is

3 mm. S2, S3, and S4 are the typical representative of high temperature and medium stress. The three sections are predicted to have a serious microstructural degradation. The direction of microstructural observation is perpendicular to the direction of centrifugal tensile stress.

3.2 The typical microstructures on the blade

The morphology of the DZ125 blade rabbet is regarded as the original microstructure in this work. Figure 4A gives the typical morphology of the blade rabbet. The γ′ precipitates are observed to be close to cuboidal and very similar to the microstructure after the standard heat treatment. The size of the γ′ precipitates is about $0.5 \pm 0.05\,\mu m$, and the volume fraction of the γ′ precipitates is about 75% ± 5%.

The representative sections are examined to show microstructural degradation in different ways mainly resulted from the gradient change in temperature and stress closely related to the geometric structure of the blade. The γ–γ′ morphology of the LEs on the five cross sections is shown in the blue box of Figure 4B. As expected, there is an obvious difference in morphologies and sizes of the γ′ precipitates, comparing with that of the DZ125 blade rabbet. S3 and S4, however, show the most obvious rafting and serious coarsening of the γ′ precipitates because of high temperature and larger stress, while S1 and S2 as well as the area in between show slight coarsening but no obvious rafting due to low stress. It should be noted that the cubic-like shapes of the γ′ precipitates at S5 seem to still keep possibly due to low temperature even though centrifugal stress at S5 is relatively high among the five examined cross sections. Temperature and stress of S4 are high among the five chosen cross sections as shown in the red box of Figure 4A. The figures in the red box of Figure 4B show that the γ′ precipitates at the LE and TE are of the most obvious degradation. According to the geometric structure of the blade, it is known that the LE is directly impacted by high-temperature gas in service, resulting in the significant increase in temperature at the LE as shown in Figure 2A. Comparing the morphologies of γ′ precipitates at the LE and TE, it can be seen that there is a slight difference in the sizes of the γ′ precipitates. The stress of the LE is comparable to that of the TE, while the temperature of the TE is lower than that of the LE. The temperature at the SS and PS is low due to film cooling compared with that at the LE and TE so that the γ′ precipitates basically maintain the cubic shape.

Along the circumferential direction of the blade, the degradation of γ′ precipitates at the LE and TE is usually severe, especially at the LE of S3 and S4. The γ′ precipitates of the SS and PS can roughly maintain the cubic-like shape on each cross section. Relatively, there is no significant difference in the morphologies of γ′ precipitates among observation points of S5. The γ′ precipitates at S1 and S2 have a certain degree of distortion on each cross section. The γ′ precipitates of the LE and TE of S3 and S4 have obviously rafting, especially at S4, where the γ′ precipitates even have a certain degree of dissolution.

Figure 4C shows the volume fraction of γ′ precipitates on the selected cross sections. It can be seen from Figure 4C that the volume fraction of γ′ precipitates at the LE varies greatly. The volume fractions of γ′ precipitates of S3 and S4 are lower than 65% while the volume fractions of γ′ precipitates of S1, S2, and S5 are close to 75%, and the volume fraction of the γ′ precipitates at the TE is also quite different. The volume fractions of the γ′ precipitates at the SS and PS are closer, about 75%. The volume fraction of the γ′ precipitates at S5 is totally higher than that of other sections. Figure 4D shows the thickness of γ′ precipitates on the selected points. It can be seen that the γ′ precipitates at the SS and PS are significantly higher than the LE and TE and this phenomenon is the most evident in S4. The thickness of γ′ precipitates at the different positions of S4 has a great change, which means that the morphology of γ′ precipitates is more sensitive to temperature than stress.

4 Discussion

During the operation, the DZ125 blade is exposed to the complicated environment of high-temperature gas and high-speed rotation. It can be predicted that the microstructural degradation mechanism of the DZ125 blade may be different from that of the standard samples under the same condition (Serin et al., 2004). The change in the volume fraction and the thickness of γ′ precipitates with temperature and stress is shown in Figure 5. It can be seen that the volume fraction of γ′ precipitates is more sensitive to temperature because it decreases significantly with the increase in temperature. In general, the influence of pressure on the equilibrium of the system can be reasonably neglected for the condensed system. For the DZ125 superalloys, temperature affects the proportion of precipitates at equilibrium, and stress, while not affecting the proportion of precipitates at equilibrium, can accelerate this process. When stress is lower than about 220 MPa, the rafting process of γ′ precipitates is very hard to achieve the thermodynamic equilibrium even if the operation lasts more than 400 h according to the study of Chen et al. (2016). It is why the change of the volume fraction of γ′ precipitates with the rising temperature is unapparent under low stress, but the volume fraction of γ′ precipitates noticeably declines once stress is higher than the critical value. At the same time, the thicknesses of γ′ precipitates would significantly change with stress. It should be accepted that the coarsening and rafting processes of γ′ precipitates are a diffusion-control one. The coupling effect of temperature and stress affects the chemical potential gradient of elements and then influences the diffusion direction of elements, finally resulting in the change in the morphology of γ′ precipitates. The previous observed phenomena are very corresponding to the calculated temperature and stress distribution on the DZ125 blade by the established models

Figure 2 shows the temperature and stress distribution of the DZ125 blade in service are significantly geometry dependent, resulting in the fact that, as shown in Figure 4, the morphologies of the DZ125 blade after service may be quite diverse (Knowles et al., 2019). It should be noted that he evolution of γ′ precipitates is essentially the result of element diffusion which is related to temperature and stress. Thus, considering the diffusion process is of great importance. According to Fick's first law and the related thermodynamic theory (the details of the theoretical derivation are given in Supplementary Material), the effects of stress and temperature on the diffusion coefficient can be obtained, as shown in Figure 6, in which the ranges of temperature and centrifugal stress are selected based on Figure 5. The curve of parameter $(\frac{D_a}{k_0 l_0^2})$ related to diffusion coefficients and σ at different temperatures is shown in Figure 6. It can be found that temperature

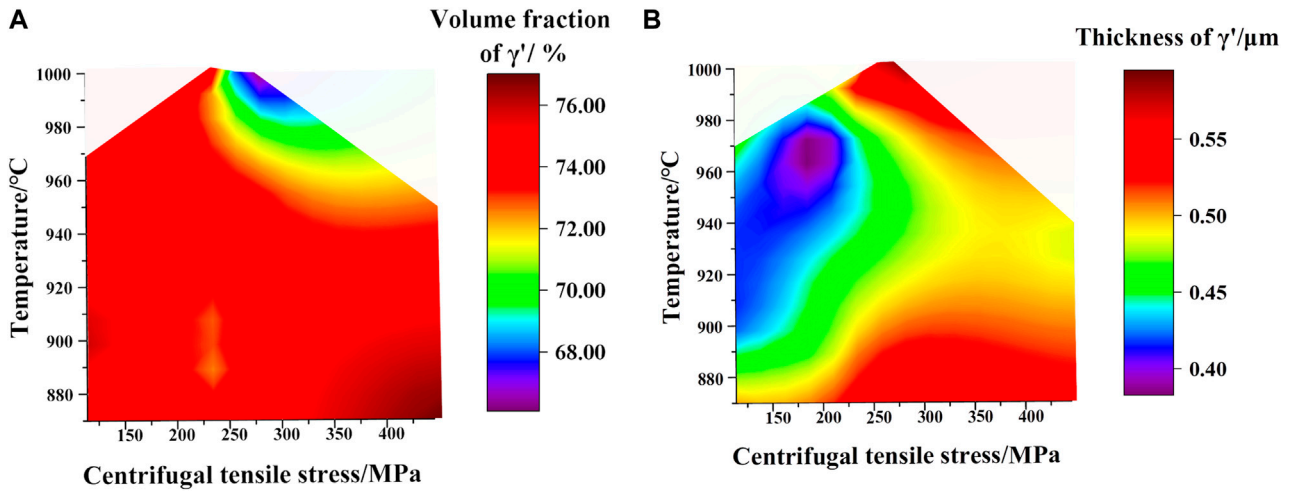

FIGURE 5
Coupling effects of stress and temperature on the configuration of γ′ precipitates in the serviced DZ125 blade. Dependence of **(A)** the volume fraction and **(B)** the thickness of γ′ precipitates on temperature and stress.

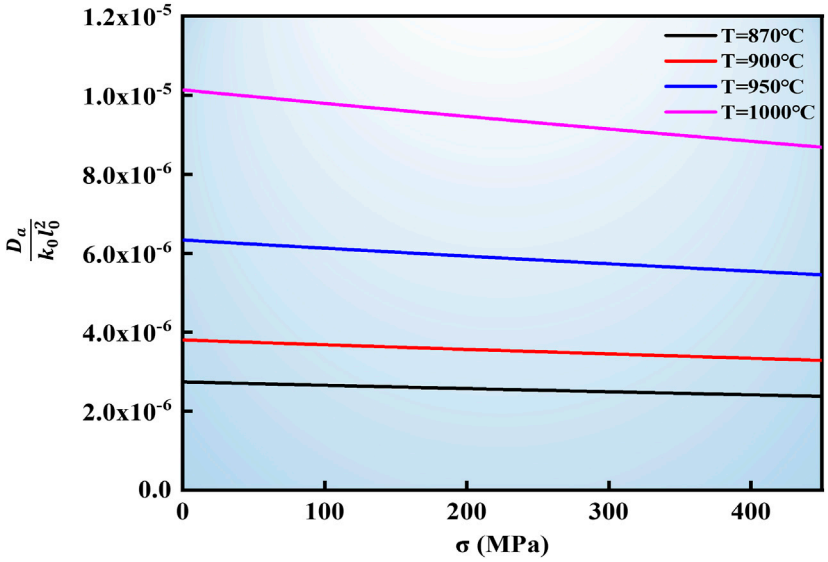

FIGURE 6
Curve of $\frac{D_a}{k_0 l_0^2}$ and σ at different temperatures for showing the coupling influence of stress and temperature on the diffusion coefficients of elements.

is the main factor affecting diffusion, and the higher the temperature is, the more obvious the influence of stress on diffusion is. Especially when temperature is more over 950 °C, the influence of stress on diffusion is very significant.

As diffusion depends on stress at high temperature, it is necessary to obtain the stress distribution at the γ–γ′ interface to evaluate the evolution of γ′ precipitates. The finite element method is used to calculate stress distribution at the γ–γ′ interface. A cubic cell containing 27 γ′ precipitates is built. The detail of the stress calculation is given in the Supplementary Material. Figure 7 shows the normalized stress distribution at the γ–γ′ interface of the DZ125 blade in service. Figure 7A gives the relationship between the corresponding stress distribution at the γ–γ′ interface with temperature. In order to compare the effects of high-speed rotation and uniaxial tensile stress on the stress distribution at the γ–γ′ interface, we keep temperature and stress values the same during the calculation, but the stress is applied in different ways, one of which is the body force (the purple area) produced by high-speed rotation and another is the surface force (the red area) produced by uniaxial tensile stress. In both cases, the stress concentration preferentially occurs at the corner of γ′ precipitates. Comparing the stress distributions at the γ–γ′ interface reveals that the stress concentration of γ′ precipitates under the body force is more obvious than the surface force. To clearly illustrate this difference, we quantitatively present the representative stress distribution curve in

10.3389/fmats.2023.1165971

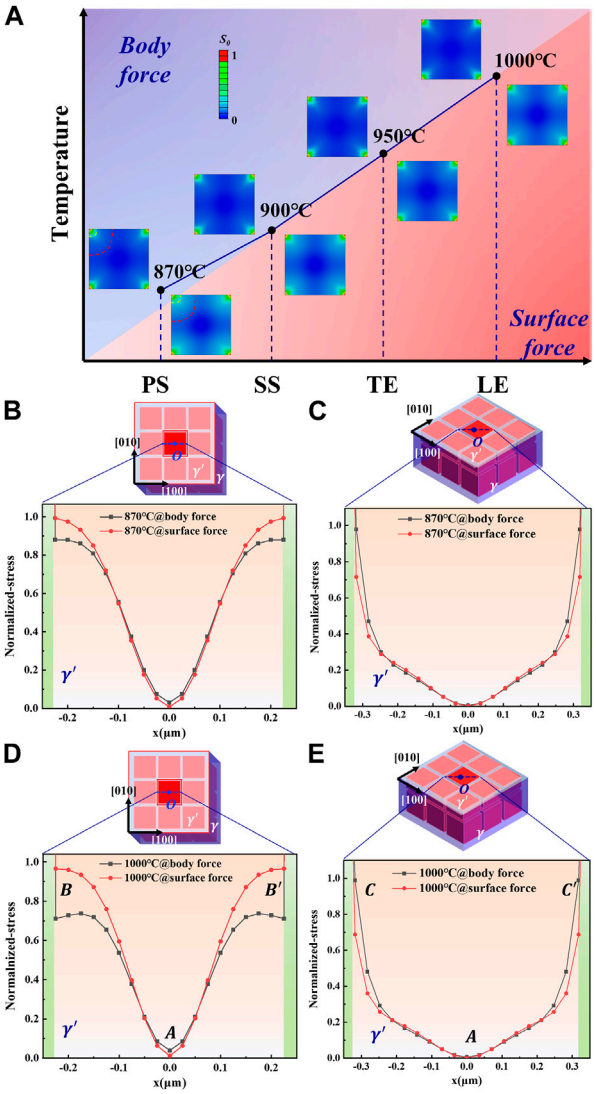

FIGURE 7
Microscopic stress distribution at the γ – γ′ interface under the surface force and the body force; **(A)** comparison of stress distribution at the γ – γ′ interface under the surface force and the body force at the same temperatures, **(B, C)** stress distribution curves on the horizontal **(B)** and diagonal **(C)** lines of γ′ precipitates at 870 °C, respectively, and **(D, E)** stress distribution curve on the horizontal **(D)** and diagonal **(E)** lines of γ′ precipitates at 1000 °C, respectively.

Figures 7B–E; Figures 7B, C show the stress distribution curve along the horizontal and diagonal lines of a γ′ precipitate at 870 °C, respectively; Figure 7B shows that the stress at the γ–γ′ interface under the surface force is about 12% higher than that under the body force. Meanwhile, on the corners of γ′ precipitates, the stress under the body force is approximately 27% higher than that under the surface force, as shown in Figure 7C. When temperature increase to 1000 °C, the stress distribution curves along the horizontal and diagonal lines of a γ′ precipitate (Figures 7D, E) reveal the similar change to 870 °C. In this case, the stress at the γ–γ′ interface under the surface force is about 27% higher than that under the body force (Figure 7D), while the stress on the corners of the γ′ precipitates under the surface force is 31% less than that under the body force (Figure 7E). These results show that even if temperature and stress values are same, the way of applying stress has an important influence on the stress distribution at the γ–γ′ interface, especially on the corners of γ′ precipitates. That is why the microstructural evolution mechanism of the DZ125 blade in this work is quite different from the standard sample under the same temperature and stress value condition.

It has been known that rafting of γ′ precipitates in Ni-based superalloys is the result of directional diffusion of elements (Guo et al., 2019b). This diffusion-dependent rafting of γ′ precipitates is closely associated with temperature and stress. According to the previous analysis of the diffusion coefficient, if the concentration gradients of elements are not considered, the diffusion rates of elements are mostly determined by temperature and stress. The diffusion direction of elements strongly depends on the gradient direction of chemical potential of elements in the studied system from the thermodynamic point of view. From Figure 2, it is a reasonable assumption that the temperature field on each observation point of each section is relatively uniform but centrifugal stress gradient cannot be ignored because of the existence of body force produced by high-speed rotation. The centrifugal stress gradient may be mainly responsible for the gradient direction of chemical potential of elements, leading to the directional diffusion of elements and accordingly causing the dependence of morphological evolution of γ′ precipitates on the centrifugal stress distribution. Nevertheless, the centrifugal stress distribution of the DZ125 blade in service is strongly dependent on its geometric structure. This is why the morphologies of γ′ precipitates at different locations on different sections of the DZ125 blade are different. Namely, the correlation between the morphologies of γ′ precipitates and the geometric structure of the DZ125 blade indirectly proves the influence of stress on the diffusion direction of elements, as shown in Figure 8.

Based on Figure 6 and the diffusion model, the model regarding the migration of the γ′-formers in the process of γ′ rafting under the body force and the surface force is built in Figure 8. According to the microscopic stress distribution of γ′ precipitates in Figure 7, there are two diffusion paths of element diffusion, as shown in Figure 8A, one of which is parallel to the side of γ′ precipitation, namely, along the B–A–B′ direction. Another path is parallel to the diagonal line of γ′ precipitation, namely, along the C–A–C′ direction. Figures 7D, E indicate that the stress in the center of the γ′ precipitates is almost zero whether under the body force or the surface force. However, compared with the stress distribution of γ′ precipitates under the surface force, the horizontal stress along γ′ precipitates is lower (~27%) and the diagonal stress along γ′ precipitates is higher (~31%) under the body force. It implies the different stress gradients derived from the body force and the surface force. More specifically, for the γ′ precipitates of the DZ125 blade under the body force, the stress gradient from A to B is 500%/μm and the stress gradient from A to C is 117%/μm. Corresponding, for the γ′ precipitates under the surface force, the stress gradient from A to B is 700%/μm and the stress gradient from A to C is 70%/μm. As shown in Figure 6B, the diffusion coefficients of elements are negatively related to stress, meanwhile, Al atoms diffuse to high-stress areas easier because the atomic radius of Al is larger than that of Ni. Combined with the stress gradient, the Al atoms are more likely to diffuse along the B–A–B′ path under the body force while along the C–A–C′ path under the surface force. It implies that the stress loading ways can change the microscopic stress distribution of γ – γ′ microstructures, causing the change of element

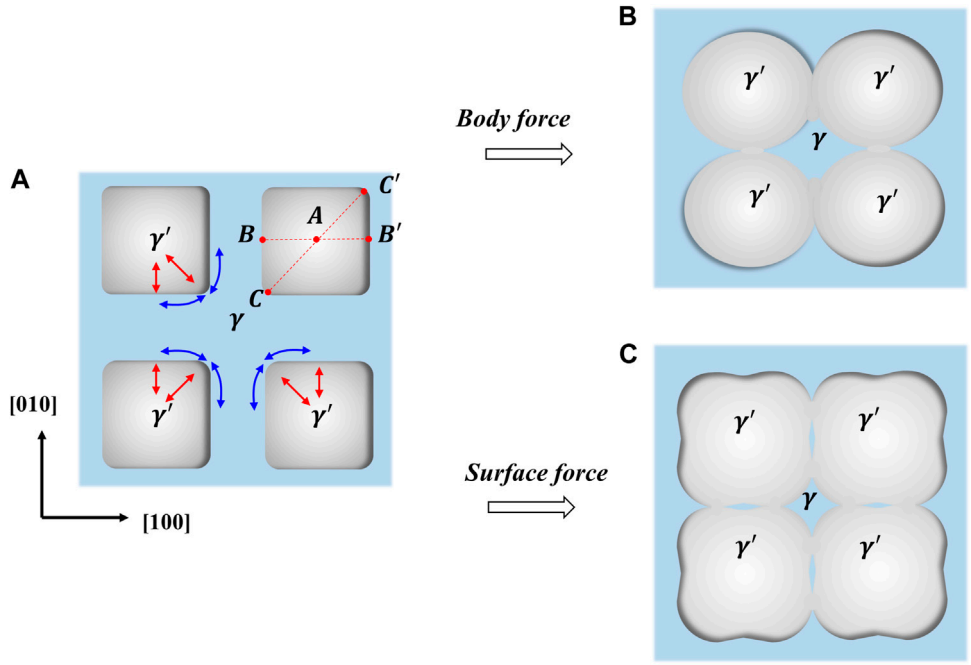

FIGURE 8
(A) Migration diagram of the γ′-formers in the process of γ′ rafting under the body force and the surface force conditions, **(B)** evolution process of γ′ precipitates under the body force, and **(C)** evolution process of γ′ precipitates under the surface force.

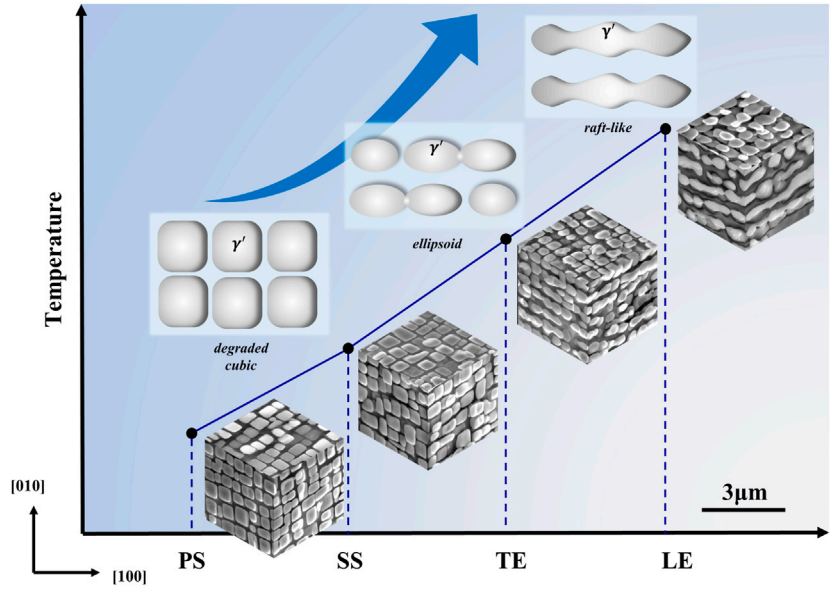

FIGURE 9
Evolution of the microstructure of the serviced DZ125 blade with temperature at S4 and the schematic of the evolution process of γ′ precipitates.

diffusion paths, and finally make the microstructural evolution in different ways. It may be the reason why there is a divergence in the evolution mechanism of γ′ precipitates on the DZ125 blade under the body force and the surface force conditions. Under the body force condition, the cubic-like γ′ precipitates tend to preferentially grow along the B–A–B′ direction in and finally occur at the priority connection of the center of γ′ precipitates as shown in Figure 8B. Under the surface force condition, the cubic-like γ′ precipitates tend to preferentially grow along the C–A–C’ direction and finally occur at the priority connection of the corners of γ′ precipitates as shown in Figure 8C.

Figure 9 gives the microstructures of each point on S4 of the DZ125 blade after service. As temperature increases, the γ′ precipitates evolve from cubic to ellipsoidal, and then, the connection occurs preferentially at the center of γ′ precipitates and finally grows into the rafted structure. It is in accordance with the microscopic stress distribution of Figure 8 and the prediction of Figure 9. Diffusion of elements is a competing process of temperature and stress. At low temperature, the diffusion coefficients of elements are low, and the rafted structure of γ′ precipitates is not apparent despite the high stress. At high temperature, the diffusion coefficients of elements are high even if stress is relatively low, and the rafted structure of γ′ precipitates was formed. This also explains why the γ′ precipitates on the DZ125 blade where the temperature is high and the stress is low also undergo obvious rafting when in service.

5 Conclusion

The directional solidified Ni-based master superalloy DZ125 was used to directionally solidify turbine blades by the Bridgman technique. The DZ125 turbine blades with the film cooling holes were operated on the engine bench with the high-temperature gas environment of more than 1500 °C from combustor and high-speed rotation of more than 13500 rpm. The microstructural evolution of the served DZ125 blades was analyzed, and the variations of microstructures with temperature and stress were investigated. The following conclusions are drawn.

A service-environment-based model was put forward to simulate the distribution of temperature and stress on the DZ125 blade in service. It was found that the distribution of temperature and stress on the serviced DZ125 blade were closely related to its geometric structure. Based on the calculated results, the LE, PS, SS, and TE locations on five sections were selected to analyze the change in the volume fraction and the size of γ′ precipitates with temperature and stress at the macroscopic level. The results indicated that temperature mainly affects the volume fraction of γ′ precipitates while stress has a principal effect on the thickness of γ′ precipitates. In addition, because temperature and stress distribution of the serviced DZ125 blade are significantly geometry dependent, the γ − γ′ morphology of the serviced DZ125 blade may be quite diverse, which is different from that of the standard sample tested at constant temperature and uniaxial tensile stress. Clearly, the stress loading way influences the microscopic stress distribution around γ′ precipitates. In order to compare the effects of high-speed rotation (the body force) and uniaxial tensile stress (the surface force) on the microscopic stress distribution at the γ–γ′ interface, a temperature–stress-based diffusion model is built and the finite-element method is used to investigate the difference in the microscopic stress distribution at the γ–γ′ interface under the body force and the surface force conditions. Comparing the microscopic stress distributions at the γ–γ′ interface reveals that the stress concentration of γ′ precipitates under the body force is more obvious than the surface force. These results show that even if the temperature and stress value are the same, the way of applying stress has an important influence on the microscopic stress distribution at the γ–γ′ interface, especially on the corners of γ′ precipitates. That is why the microstructural evolution mechanism of the DZ125 blade in this work is quite different from the standard sample under the same temperature and stress value condition. A combination of the calculated stress distribution and the diffusion coefficients of elements is used to explain the formation of the rafted structure of γ′ precipitates on the serviced DZ125 blade for 400 h. It means that diffusion of elements during the rafting process of γ′ precipitates is a competing process of temperature and stress. Based on a temperature–stress-based diffusion model, the calculated results show the diffusion coefficients of elements are low at low temperature, and the rafted structure of γ′ precipitates is not apparent despite the high stress. At high temperature, the diffusion coefficients of elements are high even if stress is relatively low, and the rafted structure of γ′ precipitates is formed. This also explains why the γ′ precipitates on the serviced DZ125 blade where the temperature is high and the stress is low also undergo obvious rafting.

Data availability statement

The original contributions presented in the study are included in the article/Supplementary Material; further inquiries can be directed to the corresponding author.

Author contributions

HW designed the experiments and supervised the project. JZ and YX performed the experiments and analyzed the data. YX and HF performed the computational simulations. YX wrote the paper. HW and HF revised the paper.

Funding

This work was supported by the Basic Science Center Program for Multiphase Evolution in Hypergravity of the National Natural Science Foundation of China (grant number 51988101) and the National Natural Science Foundation of China (grant number 52173302).

Conflict of interest

The authors declare that the research was conducted in the absence of any commercial or financial relationships that could be construed as a potential conflict of interest.

Publisher's note

Supplementary material

The Supplementary Material for this article can be found online at: https://www.frontiersin.org/articles/10.3389/fmats.2023.1165971/full#supplementary-material

References

Barba, D., Alabort, E., Garcia-Gonzalez, D., Moverare, J. J., Reed, R. C., and Jerusalem, A. (2018). A thermodynamically consistent constitutive model for diffusion-assisted plasticity in Ni-based superalloys. *Int. J. Plasticity* 105, 74–98. doi:10.1016/j.ijplas.2017.12.007

Chellali, M. R., Zheng, L., Schlesiger, R., Bakhti, B., Hamou, A., Janovec, J., et al. (2016). Grain boundary segregation in binary nickel–bismuth alloy. *Acta Mater.* 103, 754–760. doi:10.1016/j.actamat.2015.11.003

Chen, B., Zhao, Z., Dong, C., and Yang, X. (2020). Initiation and early-stage growth of internal fatigue cracking under very-high-cycle fatigue regime at high temperature. *Metallurgical Mater. Trans. A* 51 (4), 1575–1592. doi:10.1007/s11661-020-05633-3

Chen, Y., Zheng, Y., and Feng, Q. C. (2016). Evaluating service temperature field of high-pressure turbine blades made of directionally solidified dz125 superalloy based on micro-structural evolution. *Acta Metall. Sin.* 52, 1545–1556. doi:10.11900/0412.1961.2016.00170

Cottura, M., Appolaire, B., Finel, A., and Le Bouar, Y. (2016). Coupling the Phase Field Method for diffusive transformations with dislocation density-based crystal plasticity: Application to Ni-based superalloys. *J. Mech. Phys. Solids* 94, 473–489. doi:10.1016/j.jmps.2016.05.016

Cottura, M., Bouar, Y. L., Finel, A., Appolaire, B., Ammar, K., and Forest, S. (2012). A phase field model incorporating strain gradient viscoplasticity: Application to rafting in Ni-base superalloys. *J. Mech. Phys. Solids* 60 (7), 1243–1256. doi:10.1016/j.jmps.2012.04.003

Duscher, G., Chisholm, M. F., Alber, U., and Ruhle, M. (2004). Bismuth-induced embrittlement of copper grain boundaries. *Nat. Mater* 3 (9), 621–626. doi:10.1038/nmat1191

Dye, D., Ma, A., and Reed, R. C. (2008). "Numerical modelling of creep deformation in a CMSX-4 single crystal superalloy turbine blade," in Proceedings of the International Symposium on Superalloys, 01 January 2008 (United Kingdom: Oxford University Press), 911–919.

Eshati, S., Abu, A., Laskaridis, P., and Khan, F. (2013). Influence of water–air ratio on the heat transfer and creep life of a high pressure gas turbine blade. *Appl. Therm. Eng.* 60 (1-2), 335–347. doi:10.1016/j.applthermaleng.2013.06.061

Fedelich, B., Epishin, A., Link, T., Klingelhoffer, H., Kunecke, G., Portella, P. D., et al. (2012). *Rafting during high temperature deformation in a single crystal superalloy: Experiments and modeling*. United States: Wiley, 490–500.

Fu, C., Chen, Y., He, S., Antonov, S., Li, L., Zheng, W., et al. (2019). ICME framework for damage assessment and remaining creep life prediction of in-service turbine blades manufactured with Ni-based superalloys. *Integrating Mater. Manuf. Innovation* 8 (4), 509–520. doi:10.1007/s40192-019-00161-4

Fu, C., Chen, Y., Li, L., Antonov, S., and Feng, Q. (2020). Evaluation of service conditions of high pressure turbine blades made of DS Ni-base superalloy by artificial neural networks. *Mater. Today Commun.* 22, 100838. doi:10.1016/j.mtcomm.2019.100838

Gan, W., Gao, H., Zhao, Y., Wen, Z., Lu, G., Jiang, B., et al. (2020). Influence of microstructure degradation induced by pretreatment on the creep behavior in Ni-based single-crystal superalloy with different orientations. *J. Mater. Res.* 35 (6), 610–622. doi:10.1557/jmr.2020.35

Guo, X., Qin, X. Y., Huang, D. W., and Yan, X. J. (2019b). Morphology evolution and probability characteristic of γ' phase in single crystal superalloy during creep rafting. *Key Eng. Mater.* 827, 373–378. doi:10.4028/www.scientific.net/kem.827.373

Guo, X., Zheng, W., Xiao, C., Li, L., Antonov, S., Zheng, Y., et al. (2019a). Evaluation of microstructural degradation in a failed gas turbine blade due to overheating. *Eng. Fail. Anal.* 103, 308–318. doi:10.1016/j.engfailanal.2019.04.021

Holländer, D., Kulawinski, D., Weidner, A., Thiele, M., Biermann, H., and Gampe, U. (2016). Small-scale specimen testing for fatigue life assessment of service-exposed industrial gas turbine blades. *Int. J. Fatigue* 92, 262–271. doi:10.1016/j.ijfatigue.2016.07.014

Huang, J., He, Z., Lyu, S., Yang, X., Shi, D., Sun, Y., et al. (2022). A physically-based representative stress methodology for predicting stress rupture life of Ni-based DS superalloy. *Chin. J. Aeronautics* 2022, 1–6. doi:10.1016/j.cja.2022.07.006

Ichitsubo, T., Koumoto, D., Hirao, M., Tanaka, K., Osawa, M., Yokokawa, T., et al. (2003). Rafting mechanism for Ni-base superalloy under external stress: Elastic or elastic–plastic phenomena? *Acta Mater.* 51 (14), 4033–4044. doi:10.1016/s1359-6454(03)00224-6

Kakehi, K. (1999). Tension/compression asymmetry in creep behavior of a Ni-based superalloy. *Scr. Mater.* 41 (5), 461–465. doi:10.1016/s1359-6462(99)00191-8

Knowles, A., Reynolds, L., A Vorontsov, V., and Dye, D. (2019). A nickel based superalloy reinforced by both Ni3Al and Ni3V ordered-fcc precipitates. *Scr. Mater.* 162, 472–476. doi:10.1016/j.scriptamat.2018.12.013

Liu, C., Zhu, H., Bai, J., and Xu, D. (2010). Film cooling performance of converging slot-hole rows on a gas turbine blade. *Int. J. Heat Mass Transf.* 53 (23-24), 5232–5241. doi:10.1016/j.ijheatmasstransfer.2010.07.036

Maldini, M., Angella, G., and Lupinc, V. (2007). Analysis of creep curves of a nickel base superalloy in a wide stress/temperature range. *Mater. Sci. Eng. A* 462 (1-2), 436–440. doi:10.1016/j.msea.2005.11.084

Pollock, T. M., and Argon, A. S. (1994). Directional coarsening in nickel-base single crystals with high volume fractions of coherent precipitates. *Acta Metallurgica Materialia* 42 (6), 1859–1874. doi:10.1016/0956-7151(94)90011-6

Rogge, T., Berger, R., Pohle, L., Rolfes, R., and Wallaschek, J. (2018). Efficient structural analysis of gas turbine blades. *Aircr. Eng. Aerosp. Technol.* 90 (9), 1305–1316. doi:10.1108/aeat-05-2016-0085

Rowe, J. P., and Freeman, J. W. (1961). *Final report to National Aeronautics and Space Administration: Relations between microstructure and creep-rupture properties of Nickel-base alloys as revealed by overtemperature exposures*. United States: University of Michigan, 149.

Sadowski, T., and Golewski, P. (2012). Detection and numerical analysis of the most efforted places in turbine blades under real working conditions. *Comput. Mater. Sci.* 64, 285–288. doi:10.1016/j.commatsci.2012.02.048

Saturday, E. G., Li, Y. G., Ogiriki, E. A., and Newby, M. A. (2017). Creep-life usage analysis and tracking for industrial gas turbines. *J. Propuls. power* 33 (5), 1305–1314. doi:10.2514/1.b35912

Sen, B., Schmidt, D. L., and Bogard, D. G. (1996). Film cooling with compound angle holes: Heat transfer. *J. Turbomach.* 118 (4), 800–806. doi:10.1115/1.2840937

Serin, K., Gobenli, G., and Eggeler, G. (2004). On the influence of stress state, stress level and temperature on γ-channel widening in the single crystal superalloy CMSX-4. *Mater. Sci. Eng. A* 387, 133–137. doi:10.1016/j.msea.2004.01.114

Shi, D., Dong, C., and Yang, X. (2013). Constitutive modeling and failure mechanisms of anisotropic tensile and creep behaviors of nickel-base directionally solidified superalloy. *Mater. Des.* 45, 663–673. doi:10.1016/j.matdes.2012.09.031

Sinha, A. K., Bogard, D. G., and Crawford, M. E. (1991). Film-cooling effectiveness downstream of a single row of holes with variable density ratio. *J. Turbomach.* 113 (3), 442–449. doi:10.1115/1.2927894

Takahashi, A., Kobayashi, Y., and Kikuchi, M. (2008). Phase field simulation of rafting behavior of γ`Phase in nickel base superalloy. *Adv. Mater. Res.* 33-37, 471–476. doi:10.4028/www.scientific.net/amr.33-37.471

Tian, S., Zhang, S., Fushun, L., Anan, L., and Jingjing, L. (2011). Microstructure evolution and analysis of a single crystal nickel-based superalloy during compressive creep. *Mater. Sci. Eng. A* 528 (15), 4988–4993. doi:10.1016/j.msea.2011.03.035

Tong, J., Ding, X., Wang, M., Yagi, K., Zheng, Y., and Feng, Q. (2016). Assessment of service induced degradation of microstructure and properties in turbine blades made of GH4037 alloy. *J. Alloys Compd.* 657, 777–786. doi:10.1016/j.jallcom.2015.10.071

Wang, S., Ditta, A., Xu, Y., and Zhang, Z. (2021). Effect of microstructures restoration on high temperature fatigue behavior of DZ125 superalloy. *Prog. Nat. Sci. Mater. Int.* 31 (4), 633–640. doi:10.1016/j.pnsc.2021.07.005

Yue, Q., Liu, L., Yang, W., Sun, D., and Huang, T. (2019). Stress dependence of the creep behaviors and mechanisms of a third-generation Ni-based single crystal superalloy. *J. Mater. Sci. Technol.* 35 (5), 752–763. doi:10.1016/j.jmst.2018.11.015

Zadvorniy, E. A., Kravchuk, L. V., Buiskikh, K. P., Kiselevskaya, S. G., Feofentov, N. N., and Lebedin, A. Y. (2015). Analysis of the material damage influence on the stress-strain state of gas-turbine engine blades. *Strength Mater.* 47 (6), 797–803. doi:10.1007/s11223-015-9716-1

Zhao, Z., Liang, Z., Li, Q., Zhang, F., and Chen, B. (2022). Crack initiation and propagation behaviour under high-temperature very-high-cycle fatigue: Directionally solidified columnar-grained vs. single-crystal superalloys. *Mater. Sci. Eng. A* 836, 142711. doi:10.1016/j.msea.2022.142711